THE JOURNAL OF PHYSICAL CHEMISTRY B

pubs.acs.org/JPCB Article

Vapor-Deposited Glasses Highlight the Role of Density in Photostability

K. Michael Salerno, Joseph L. Lenhart, Juan J. de Pablo,* and Timothy W. Sirk*

Cite This: J. Phys. Chem. B 2020, 124, 6112–6120 Read Online

ABSTRACT: Photoresponsive molecules can be integrated into glassy materials to probe the local environment and invoke responsive changes in polymer behavior. For example, recent experiments and simulations have studied increased stability in vapor-deposited glasses by examining the photoisomerization rate of a probe molecule. At the theoretical level, past work relied on coarse-grained simulations to explain the role of photoisomerization on glass behavior. In order to effectively exploit these molecular probes, an ability to quantify how the local environment influences the photoisomerization rate is needed. In this work, we present all-atom molecular-dynamics (MD) simulations of molecular glasses of photoresponsive azobenzene (AB) molecules. The stability of these in-silico samples is probed using photoisomerization, where AB molecules can undergo trans → cis transition upon light exposure. Vapor-deposited and bulk-cooled glasses of AB are simulated using a classical dihedral-switching potential developed by Böckmann et al. (*J. Phys. Chem. A* **2010**, *114*, 745−754) to model the photoisomerization process. The MD simulations include thousands of molecules and run for tens of nanoseconds. These size and time scales allow us to explore the broad distribution of photoisomerization wait times, which yields two results. First, the wait-time distributions for both physical vapor deposition and bulk-cooled glasses depend strongly on sample and local density, showing that density or local packing is a primary factor in glass stability against photoisomerization and the experimentally measured photoresponse. Second, the distribution follows a power-law with exponent $b \approx 1.25-1.3$ that extends to longer times with increasing density. The power-law distribution suggests a connection with previous experiments that related barriers to photoisomerization with an effective photoisomerization temperature.

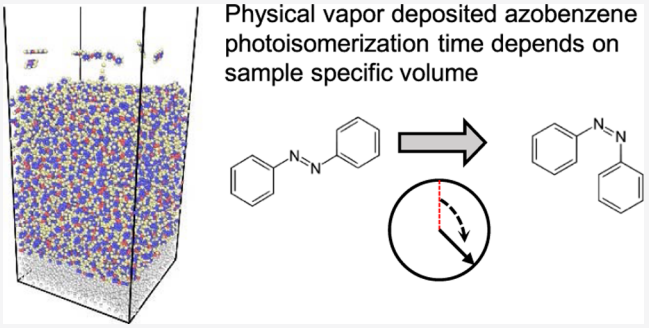

INTRODUCTION

A little over a decade ago it was discovered that "tuning" the substrate temperature during physical vapor deposition (PVD) can yield ultra-stable glasses.[1,2] Multiple features of these materials have now been uncovered. In particular, experiments on PVD glasses have found lower enthalpy, higher modulus, higher molecular anisotropy, and increased density and photostability relative to bulk-cooled glasses.[1−5] Computer simulations of the PVD process replicate the same increased glass stability.[6,7] The anisotropy, increased density, and photostability found in experimental glasses are all features of simulated glasses as well.[5,8−10] In addition, lower inherent structure (IS) energy, which is linked to lower mobility, can be measured in the "in silico" PVD glasses.[11] Simulated and experimental glasses made through PVD have used the deposition substrate temperature to open new realms of study through denser, more stable glass samples.

Recent experiments and simulations have documented the tenfold increase in the stability of photoresponsive molecules in a molecular glass[9] or glass mixture[5] created using PVD. These studies show dramatic changes in the photoresponse rate with small changes in density and highlight the need to understand how photoisomerization can be quantitatively linked to local density. Photoisomerization has been used to study how local free volume in polymer glasses varies with the location (i.e., backbone or side chain),[12,13] across polymer matrix types,[12,14,15] with physical aging,[16] curing, or hydrogen bonding.[15,17] In addition, the size of the photochromic probes and their isomerization mechanism has also been a useful tool to study changes in free volume in glassy polymers, with significant differences in the isomerization rate linked to the probe-molecule size[14,18] and isomerization mechanism.[18]

Free-volume fluctuations have long been linked to structural and dielectric relaxation in glassy solids.[19] Many early experimental works[15,18,20,21] interpreted slow photoisomerization dynamics using a theory linking free-volume relaxation with a particular distribution of free volume values.[22] Recently, experiments measured a power-law tail in the orientation

Received: April 22, 2020
Revised: May 28, 2020
Published: June 17, 2020

https://dx.doi.org/10.1021/acs.jpcb.0c03579
J. Phys. Chem. B 2020, 124, 6112–6120

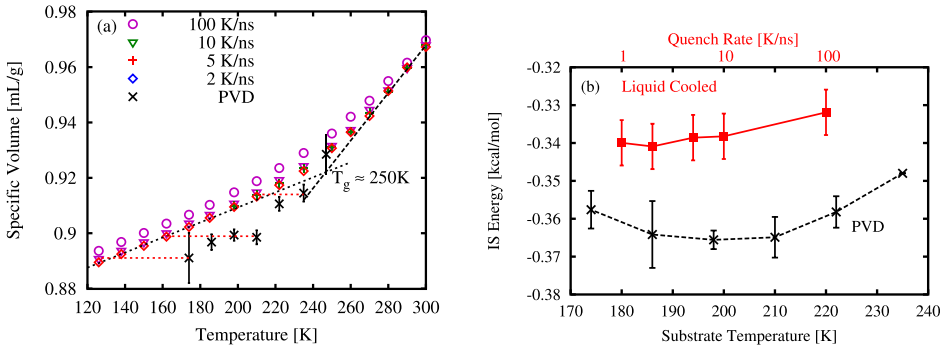

Figure 1. (a) Specific volume of AB samples as a function of temperature for quench rates from 2 to 100 K/ns. For bulk-cooled samples symbols indicate the cooling rate and uncertainties are slightly smaller than the symbol size. Fit lines to the low- and high-temperature ranges for the $\dot{Q} = 2$ K/ns are shown, and their intersection at $T_g \approx 250$ K is our estimate of the glass transition temperature. For PVD samples, indicated with × symbols, the uncertainties shown are determined by binning the PVD sample by height. For PVD systems, the temperature indicates the substrate temperature. (b) Per-atom potential energy of the IS for AB samples with different bulk-cooled rates (red) and PVD substrate temperatures (black). Note the logarithmic scale (top) for quench rate and linear scale (bottom) for substrate temperature.

relaxation of photoresponsive molecules, then related the power-law exponent with an effective photoisomerization temperature.[23] Other recent work on identifying structural or free-volume defects in amorphous materials suggests that such flow defects may move diffusively in an effective relaxation or flowability space.[24]

There are relatively few simulations of photoresponse within a polymer or molecular glass. Recent exceptions have used lattice-based Monte-Carlo approaches to model glasses[25] or tethered molecules.[26] This gap is largely due to the difficulty of simultaneously modeling a large number of high-molecular weight molecules and the quantum-mechanical photoactivation process. The approach taken here is to use a continuous, ab initio-derived activation potential to model the azobenzene (AB) photoactivation.[27,28] Previous work in this direction has allowed significant bridging of scales when all interactions can be computed in a classical molecular-dynamics (MD) framework.[29−31]

The goal of our work here is to contribute additional molecular-level information to the previous experimental work that linked the photoisomerization dynamics to a variety of polymer-glass features. More specifically, molecular-level data could lead to a better understanding of the realizable bounds in creating and engineering responsive materials. The remainder of the paper is structured as follows: first, details of the simulation models and the details from the PVD and bulk-cooled glass-preparation and photoactivation simulations are given. Photoactivation simulation results are then presented that link the isomerization wait time with the sample preparation and temperature. Features in the local density and potential energy that correlate with the wait time are then presented. Lastly, we discuss our conclusions drawn from the work and future research directions.

SIMULATION METHODS

Potential and Force Field. Simulations of our AB molecular glasses were carried out using the OPLS-AA force field with some modifications to be consistent with the GROMOS force-field[32] used in previous work on the force-field parameterization of AB.[27,33] The photoactivation process is represented by a switchable classical dihedral potential developed in the same work. The atoms within the azo group are the locus of the photoactive behavior, and the activated potential is based around the C−N═N−C dihedral. In this model, the dihedral energy is represented by a function of the dihedral angle φ. The φ potential approximates the energy from ab initio calculations. In addition, parameters for each of the bond, bond-angle, dihedral, and improper-dihedral interactions that involve one or more carbon or nitrogen atoms are also modified from the standard GROMOS force-field values, and the interaction parameters themselves depend on the value of the dihedral angle φ. The full set of interaction parameters is given in Table 1 of Böckmann et al.[28] It is important to note that the phenomenological potential used here only represents the first-order excitation and relaxation effects, and that for the long isomerization wait times that we observe, secondary effects such as radiative decay or other transitions could become important.

Simulations were performed with the LAMMPS MD simulator.[34] A modified code-base was used to implement the classical activated dihedral switching potential of Böckmann et al.[28] A 1 fs timestep was used. Coulomb interactions were computed using the particle−particle particle−mesh method.[35]

Sample Preparation. Simulations of the bulk-cooled AB molecular glass contain 4096 molecules (98,304 atoms) and are periodic in the x, y, and z-directions. Bulk-cooled samples were prepared using a constant-pressure quench at 20 atm. The pressure and temperature are controlled by a Nosé−Hoover barostat with a pressure time constant of 1 ps and a thermostat with a time constant of 0.1 ps. For bulk-cooled samples, the quench rate $\dot{Q}$ was varied more than an order of magnitude from $\dot{Q}$ = 100−2 K/ns. Although AB readily crystallizes, our focus is on isomerization dynamics in disordered environments, and to this end, we deliberately did not strive for low quench rates where crystalline samples could occur. Figure 1a shows the specific volume of the samples for several cooling rates. Data from PVD simulations, which will be described below, are also shown.

We calculate the glass transition temperature T_g as the point of intersection of extrapolated linear fits to the high- and low-temperature regimes shown in Figure 1a. The value of T_g is approximately 250 K. For each of the cooling rates, except $\dot{Q}$ = 2 K/ns, multiple independent systems were cooled and uncertainties for each of the points were calculated. The largest uncertainty occurs for $\dot{Q}$ = 100 K/ns just above T_g with an absolute value of ±0.0015 mL/g, slightly smaller than the figure symbols. Despite the importance of density or volume to

https://dx.doi.org/10.1021/acs.jpcb.0c03579
J. Phys. Chem. B 2020, 124, 6112−6120

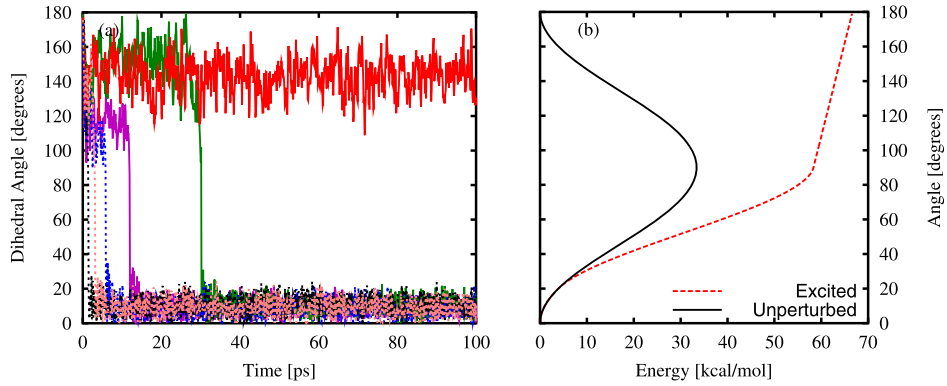

Figure 2. (a) Typical time-evolution for the dihedral angle of molecules after photoactivation at time $t = 0$. Dashed lines represent samples at 235 K while solid lines are at 138 K. The slowest molecule to isomerize (solid red) isomerizes after about 10 ns. Both samples were cooled at a rate $\dot{Q} = 2$ K/ns. (b) Unperturbed and excited dihedral potential.

photoresponse time, in the remainder of the paper we refer to samples by the preparation protocol and temperature rather than (inverse) density because different sample preparation/temperature pairs can lead to the same sample density, that is, the density or specific volume is not uniquely determined.

PVD Sample Preparation. PVD samples are prepared by a cycle of inserting, depositing, and cooling molecules similar to the process described by Qiu et al.[9] PVD samples were grown to a size of approximately 2000 molecules. The simulation cell has a 7 nm × 7 nm periodic cross section in the x and y-directions and a height of 15.0 nm < L_z < 25.0 nm in the direction normal to the deposition substrate. The AB molecules were initially deposited on an amorphous substrate with height ≈1.5 nm composed of particles with Lennard–Jones interactions $\sigma = 0.3$ nm and interaction strength $\epsilon = 1.1$ kcal/mol. Throughout the simulations, the substrate atoms remained tethered to their initial positions using harmonic springs with substrate temperature T_s using an NVT thermostat with a time constant of 0.1 ps.

A simulation cycle replicates the experimental PVD process. A small number (5–10) of AB molecules are introduced in a region between 0.6 and 2 nm above the highest point in the sample. They are imparted with velocity consistent with a temperature $T = 350$ K, well above the glass transition temperature, and a small velocity bias toward the substrate. Molecules are constrained to the volume near the substrate and PVD sample by a reflecting barrier at the top of the simulation cell. The temperature of the inserted molecules is maintained at $T = 350$ K for 200 ps, and then the temperature is reduced from $T = 350$ K to T_s over 1.2 ns, followed by 200 ps at T_s. Substrate temperatures are 174, 186, 198, 210, 222, 234, and 247 K. After this quench sequence, new deposition molecules are inserted in the simulation and the cycle repeats. The results presented here are from PVD samples built up over 250–300 molecule insertion cycles. This number of cycles leads to samples where the sample thickness is sufficient to produce an interior "bulk-like" region away from the free surface and substrate. Molecules from this region can be compared with the bulk-cooled samples, which contain no substrate or free surface. Data on the specific volume and molecular mobility through the PVD samples can be found in the Supporting Information.

The sample specific volume data for PVD AB samples are shown in Figure 1a. For the PVD samples, the specific volume uncertainties are significantly larger than bulk-cooled samples because we are limited to a single sample for each substrate temperature. Uncertainties were determined by binning the PVD samples by height and analyzing the specific volume at each height value. More information can be found in the Supporting Information.

Inherent Structure. In MD simulations, analysis of the local potential-energy minima has proved useful in many systems, and these PE minima have been termed ISs.[36−38] Previous computational studies have shown that the IS energy is a good indicator of the stability of both PVD and bulk-cooled glass and is linked to the local dynamics.[11] Here, we use the IS energy to compare our glass samples and confirm the increased stability of PVD samples relative to bulk-cooled samples.

Figure 1b shows the IS energy of bulk-cooled samples (red squares) on a logarithmic cooling-rate scale. The IS energies for PVD samples are represented in black as a function of the substrate temperature along the bottom axis of Figure 1b. For both the bulk-cooled and PVD systems, the IS energy is calculated from a common temperature $T = 186$ K by quenching the sample to $T = 0$ using the fast inertial relaxation engine as implemented in LAMMPS.[39] AB PVD samples are heated or cooled to 186 K at a rate of 2 K/ns, while applying a strain rate $\dot{\epsilon}_{xx} = \dot{\epsilon}_{yy} \approx 2 \times 10^{-4}$/ns to match the thermal expansion of the glass in Figure 1. The PVD samples show a characteristic minimum in the IS energy at about $0.8T_g = 200$ K.[5,40] The sample at $T_s = 210$ K also has the lowest specific volume relative to the bulk-cooled samples. For all substrate temperatures, the IS energy is substantially less than for the bulk-cooled samples. In fact, assuming a logarithmic dependence on the cooling rate, the effective cooling rates for the PVD samples range from 2 to 4 orders of magnitude slower than the bulk-cooled sample at our lowest rate. For comparison, k_BT at 200 K is approximately 0.4 kcal/mol.

Activation-Response Simulations. One over-arching goal is to correlate structural properties of a glass sample, such as the IS energy or the local density, with the experimentally measured photoresponse. From the PVD simulations, we save snapshots where the sample thickness of approximately 10 nm yields a region free from effects of the free surface or the substrate. See the Supporting Information for details. These PVD "bulk"-like regions are compared with results from snapshots from the bulk-cooled samples. From these two types of glass samples, we initiate many independent simulations, each with the dihedral interaction for a single AB

https://dx.doi.org/10.1021/acs.jpcb.0c03579
J. Phys. Chem. B 2020, 124, 6112−6120

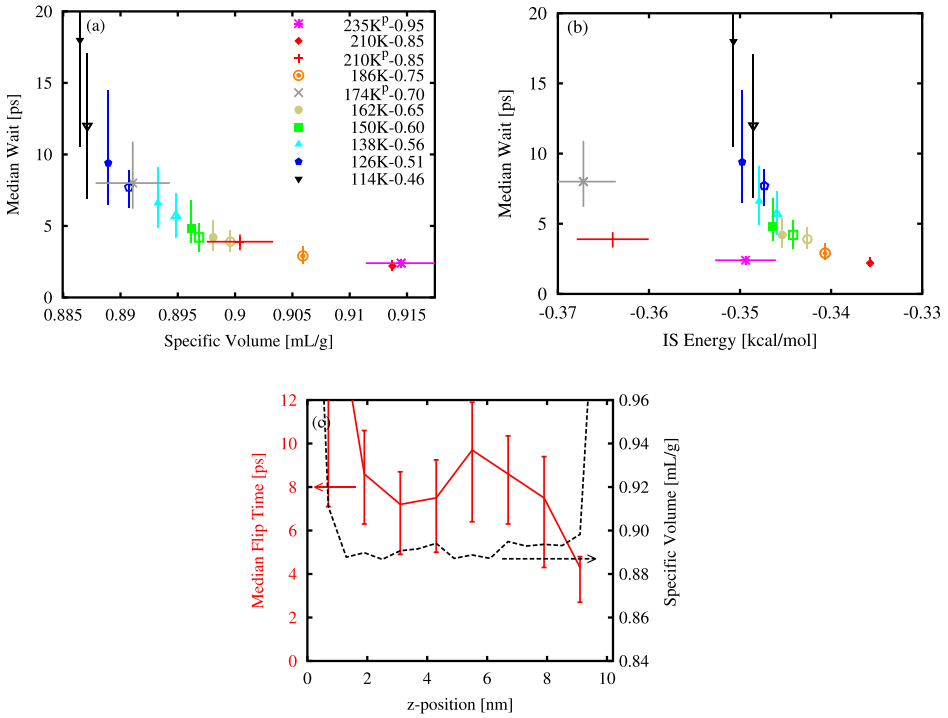

Figure 3. (a) Median wait time versus the specific volume for bulk-cooled and PVD AB systems. Symbol types represent different temperatures, with open (closed) symbols representing systems with 10 K/ns (2 K/ns) cooling rate. PVD samples are indicated by ^{P} in the legend. (b) Median wait time versus the IS energy for the same systems as in (a). Vertical error bars indicate the middle 10% of wait times, while horizontal error bars indicate specific volume or IS energy variations within the PVD samples. (c) Median wait time (solid red, left axis) and AB specific volume (dashed black, right axis) as a function of position through the PVD sample at 174 K. The substrate is located at $z = 0$ nm and is omitted from the specific volume calculation, while the free surface is at $z \approx 10$ nm.

molecule activated, and all other interactions unchanged. This process mimics photoactivation of dilute molecules in a nonabsorbing matrix, where the light penetration depth is larger than the dimension of the sample. These simulations are all performed in the NVE ensemble, retaining the molecular volume and temperature from the quench or PVD snapshot. During the simulation, the angle of the activated dihedral is monitored and the simulation is ended after a dihedral-angle rotation past 90° is detected.

For our bulk-cooled AB, there are 4096 independent simulations, corresponding to the number of molecules in each sample. For the PVD AB samples, the intermediate region is roughly 7 nm × 7 nm × 5 nm, corresponding to about 1000 molecules and independent simulations. During these simulations, data for the atomic positions, velocities, and forces are available from the activation at time $t = 0$ through a time 50–100 ps after the dihedral passes 90°. Typical time-traces of the dihedral-angle φ for AB at two different sample temperatures are shown in Figure 2a. We define the dihedral "flip" time t_f as the time when the dihedral angle passes through $\varphi = 90°$. The value $\varphi = 90°$ corresponds to a sharp drop in the excited dihedral potential, as seen in Figure 2b, that leads to large forces on the dihedral atoms for these angle values. The statistics of t_f are of significant interest, showing wide variation and a strong specific volume dependence. This quantity is the microscopic quantity which, with a fully-characterized distribution, produces the experimental photoactivation rate.

RESULTS AND DISCUSSION

Isomerization Time Scale. Previous work has shown that the timescale for photoisomerization within a rigid solid is both broad, spanning minutes or hours,[18] and sensitive to small changes in the confining matrix.[5] The measured photoisomerization wait-time distributions are presented in detail below, but here we present results for the distribution median for different system preparations and states. We focus on the median value because it is experimentally convenient to measure when a particular fraction of photoresponsive molecules has isomerized. Further, for broad distributions, moments may depend on the largest observed values and are difficult to calculate when simulations are restricted by a finite cpu walltime. The corresponding results for the distribution mean, which are heavily influenced by the distribution tail, are presented in the Supporting Information.

Figure 3a shows the median wait time as a function of the system specific volume for AB molecular glass samples. Samples with different temperatures and cooling-rate preparations are shown. Symbol types represent different sample temperatures, with open (closed) symbols for 10 K/ns (2 K/ns) cooling rate or PVD preparation, as indicated in the figure legend. Symbol colors also represent different temperatures, with approximate correspondence between the symbol color and T/T_g. One striking conclusion from the data is that, to a large degree, the median wait time depends on specific volume, collapsing onto a single curve for different temperatures, cooling rates, and preparation methods.

In contrast, Figure 3b shows several distinct curves for the median wait time versus IS energy. The PVD data are clearly separated from the bulk-cooled systems, showing a much lower IS energy for the same median wait time. There is also a small but clear shift in data for different cooling rates. Both these

https://dx.doi.org/10.1021/acs.jpcb.0c03579
J. Phys. Chem. B 2020, 124, 6112−6120

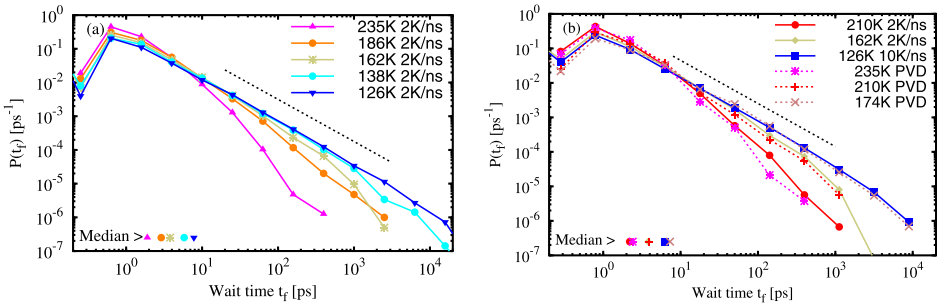

Figure 4. (a) Distribution of wait times $P(t_f)$ for bulk-cooled AB glass samples cooled at $\dot{Q} = 2$ K/ns at different temperatures. (b) Distribution of wait times $P(t_f)$ for PVD and bulk-cooled AB samples. System pairs with matching symbols have approximately equal densities.

features indicate that the differences in the IS energy do not drive the differences in photoresponse time.

Figure 3c shows the specific volume and median isomerization time as a function of height through the 174 K PVD sample. The PVD sample is divided into slabs spaced 0.6 nm, and within each slab the specific volume and median isomerization time are calculated. To improve the isomerization-time statistics, the slabs are overlapping so that each slab has a total height of 1.8 nm. Error bars represent the 45 and 55% value in the isomerization time distribution for each slab. We note the correlation of the local specific volume with the median isomerization time, particularly near the free surface, where the volume increases and the wait time decreases. At the substrate surface (near $z = 1$ nm), the immobility of the substrate atoms induces a confinement of the AB molecules and leads to the increase in the median flip time.

Using data from both the bulk-cooled and PVD samples, the median isomerization-time is linked to the sample specific volume. Further, because both the PVD and bulk-cooled samples collapse on the same wait time-specific volume curve, it is clear that in this regime specific volume, rather than IS energy or temperature, drives shifts in the wait-time distribution. Altogether, these results illustrate a very clear connection between wait time and specific volume at the sample level, in agreement with previous observations.[5] Having established the importance of the sample specific volume to the median wait time, we next look at the full wait-time distribution to see how changes in temperature, specific volume, and preparation influence the isomerization wait-time distribution.

Wait Time Distributions. The wait time t_f between the photoactivation and isomerization depends strongly on the preparation and state of the glassy sample. For both the bulk-cooled and PVD glasses, we record the wait time for each photoactive molecule and study variations in the distribution of wait times with specific volume and temperature.

Figure 4a shows the probability distribution $P(t_f)$ of wait times t_f for photoactivated molecules in bulk-cooled molecular AB glasses. The distribution of wait times becomes broader with decreasing temperature or molecular volume, increasing the breadth of the distribution by 2 orders of magnitude over the range of ∼100 K. Similarly, the median distribution value increases by almost an order of magnitude over this temperature range, while the mean value increases by over 2 orders of magnitude. For the lowest temperatures, the wait times span more than four decades, from a fraction of a picosecond to tens of nanoseconds. There is a clear power-law distribution of wait times that develops with decreasing specific volume (decreasing temperature). The slope of the distribution is $b \approx 1.25$, shown as a dashed line in Figure 4a.

Figure 4b shows the wait time distribution $P(t_f)$ for AB PVD samples developed at different substrate temperatures from $T_s = 174$ K to $T_s = 235$ K. Each PVD sample contains approximately 1000 molecules within the central "bulk" region. The effect of substrate temperature on the wait time is visible, and follows the change in the sample specific volume seen in Figure 1, with a pronounced widening of the wait time distribution that coincides with a decrease in molecular volume near $T = 0.85T_g$. Also shown are wait-time distributions for bulk-cooled AB samples that are chosen to be volume-matched with each PVD sample. For each pair of corresponding symbols, the sample specific volume is approximately equal. Despite temperature differences of 20−50 K, which correspond to as much as $T_g/4$, the match between the distributions at a common specific volume is striking.

One notable recent experiment used polarized light to manipulate order in surface-tethered, azo-containing molecules. The measured birefringence (related to order) decayed according to a power law for long times during both thermal and photoinduced relaxation.[23] The change in birefringence results from (dis-)alignment of the molecules, which is related to the integral of the wait time distribution measured here. The experimental work assumed an Arrhenius thermal relaxation over a barrier with time scale (inverse rate) $\tau \sim \exp(U_b/k_BT)$ and a distribution of barrier heights U_b that contains an exponential cutoff $f(U_b) \sim \exp(-U_b/U_m)$ and characteristic scale U_m. With these two assumptions, a change of variables yields a power-law distribution of barrier crossing times $\tilde{f}(\tau) \sim \tau^{-(b+1)}$, with exponent $b = k_BT/U_m$, the ratio of the temperature to the characteristic barrier-height energy. By comparing the experimentally observed thermal relaxation power-law exponent with the photoinduced relaxation exponent, the researchers concluded that in their experiments photoactivation induced an effective "temperature" of about 800 K. Coupling this estimate with our slope exponent of $b \approx 1.25$ gives a characteristic barrier height $U_m/k_B \approx 3200$ K or 6.4 kcal/mol. A similar analysis was also used several decades earlier, with free volume assumed to be linearly related to the energy barrier height.[18] These experiments also measured slow, long-tailed dynamics. An interesting future research avenue will be to test the assumptions of a single characteristic barrier-height and an exponential distribution.

The power-law form of the wait time distribution $P(t_f) \propto t_f^{-b}$ with exponent $b \approx 1.25$ justifies our choice to measure the distribution median above. The mean wait time $\langle t_f \rangle = \int_0^\infty P(t_f)\, t_f\, dt_f$ depends strongly on the cutoff of the distribution $P(t_f)$. With decreasing temperature it becomes more difficult to

https://dx.doi.org/10.1021/acs.jpcb.0c03579
J. Phys. Chem. B 2020, 124, 6112−6120

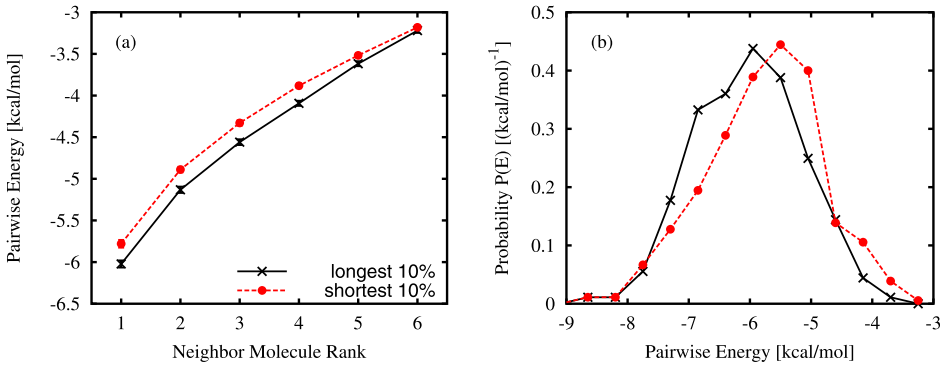

Figure 5. (a) Pairwise potential energy between a photoactivated molecule and its neighboring molecules in the ascending rank order for AB at 138 K cooled at $\dot{Q}$ = 2 K/ns. Points represent the mean. Error bars are smaller than the symbols and represent the standard error of the mean for molecules with the shortest or longest 10% of wait times. (b) Distribution of pairwise energies $P(E)$ for the longest and shortest 10% of wait times for photoactivated molecules.

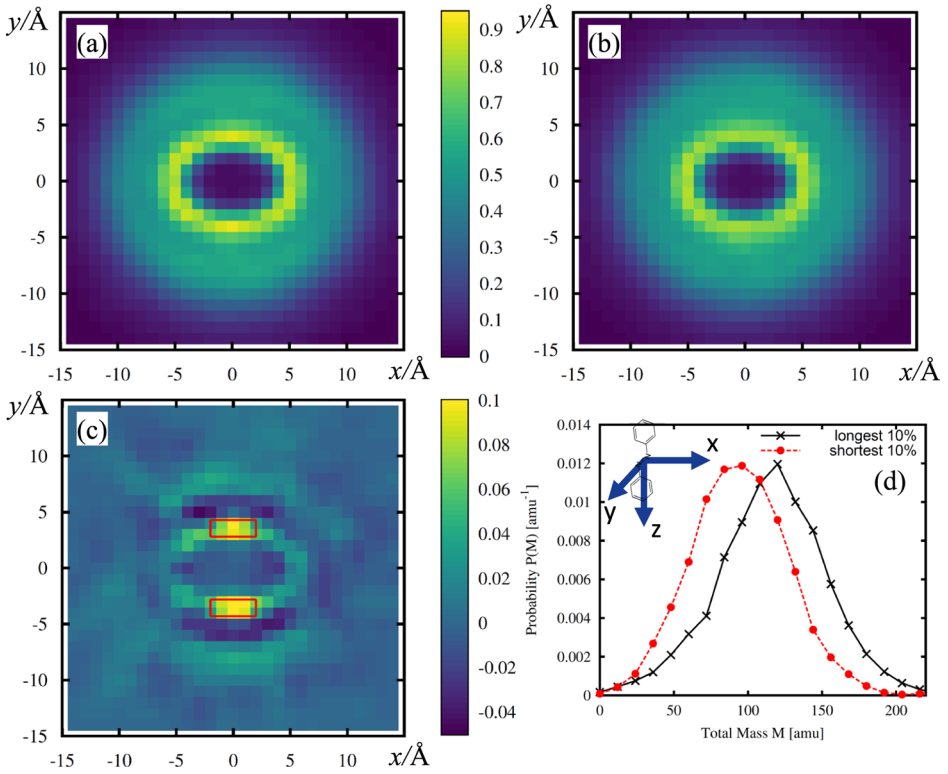

Figure 6. Local density for "long" (a) vs "short" (b) wait time isomerization events. Results are averaged over local configurations that produce the (a) longest and (b) shortest 10% wait times and are averaged over the length of the molecule in the z-direction. (c) Difference between the averaged local configurations for "long" and "short" events. Colorbars indicate the density in units of amu/Å^3. (d) Distribution of mass values within the boxed region from (c) 2.8 Å < |y| < 4.3 Å and |x| < 2 Å for long and short events. Inset (d) shows the orientation of the AB molecule relative to the axes in (a−c).

measure this cutoff, as an increasing number of molecules do not isomerize during a finite simulation time.

Local Environment. Several previous experimental efforts have used photoresponsive molecules as probes of the local environment.[12,14−18] MD simulations are well suited for characterizing the link between the local environment and the photoresponse time. Below, we examine two measures of the local structure, the local density and the local intermolecular interaction energy. Both are correlated with longer isomerization wait times.

Intermolecular Potential Energy. The potential energy is an important scalar quantity that encodes information about both local atomic configurations and interactions. Figure 5 shows the average pairwise interaction energy between photoactivated molecules and their strongest interacting neighbor molecules. In Figure 5a, the interaction energies are numerically ranked from strongest to weakest. The data are averaged over the 10% AB molecules with the largest or smallest t_f values. Because the distribution of t_f is so broad, the largest 10% of values are 4−5 orders of magnitude larger than the smallest 10%, from a fraction of a picosecond to tens of nanoseconds. Data from an AB molecular glass ($\dot{Q}$ = 2 K/ns, T = 138 K) are shown. Error bars represent the standard error of the mean. At this population level, it is clear that long and short events are distributed about different mean values. The difference in the mean is about $k_BT \approx 0.3$ kcal/mol. Events

https://dx.doi.org/10.1021/acs.jpcb.0c03579
J. Phys. Chem. B 2020, 124, 6112−6120

with large t_f values have larger (negative) pairwise interactions, indicating a more stable local environment.

However, when the pairwise molecular PE values are examined for individual environments it becomes clear that the change in the PE associated with a dramatic change in the wait time is small compared with the width of the distribution of PE values. For example, Figure 5b shows the entire distribution of the lowest PE pairwise interaction (i.e., the molecule-ranked 1 in Figure 5a) for the long and short populations of the AB sample. The width of the distributions, as characterized by the standard deviation of the population, is approximately $\sigma \approx 1$ kcal/mol, which is significantly larger than the difference of their mean values, ≈0.3 kcal/mol. Thus, while it is possible, given enough samples, to distinguish the long and short populations PE distributions, it is not possible to consistently predict, given a single PE interaction value, which population it belongs to. The statement also holds for each of the other neighbor molecules.

Local Density. Figure 6 shows colormap images of the local density around an activated AB molecule, averaged over (a) long and (b) short wait time populations. These populations represent molecules with the longest or shortest 10% of wait times for the whole wait time distribution. These short or long events are drawn from seven different system realizations at T = 138 K or T = 126 K and each figure represents 2800 local environments. The local configuration at time t = 0 is used, just before the dihedral potential is first activated. Each molecule has been oriented with its long axis aligned perpendicular to the page and rings oriented in the y = 0 plane, as in the inset diagram. Densities have been averaged along the length of the molecule in the z-direction. The local density ρ_j is computed at each point j on a 3-dimensional grid with spacing dL by summing the mass of each atom m_i in the simulation with a gaussian weight $\rho_j = \pi^{-3/2} l^{-3} (\mathrm{d}L)^{-3} \sum_i m_i \, e^{-|\mathbf{r}_i - \mathbf{r}_j|^2/l^2}$. The gaussian width l = 1 Å and $|\mathbf{r}_i - \mathbf{r}_j|$ represents the distance between the atom i and the grid point j. The alignment of the photoactivated molecules naturally leads to an elliptical shape in the density colormaps seen in Figure 6.

There are two significant features in the density maps in Figure 6a,b that are prominent in the difference image (c), which simply represents the density values in (b) subtracted from the density values in (a). The two features relate to the clearly defined ellipse of high-density material around the activated molecule. First, it appears that for the long wait time population (Figure 6a), the high-density ring is shifted closer to the activated molecule (smaller $|y|$). Second, sharper features occur in the vicinity of (0, ±3.5) but not in the region (±5, 0). Using these visual clues, we use the regions 2.8 Å < $|y|$ < 4.3 Å and $|x|$ < 2 Å as the focus of our analysis below. The region is marked with a red box in Figure 6c. When viewed along the x- and y-axis, the high-density regions marked in Figure 6c are significantly less pronounced. These colormap figures are shown in the Supporting Information.

Having identified important density regions for distinguishing photoactivation wait time, we would like to determine if these local regions can predict the photoactivation wait time. For simplicity, we use a scalar value, the sum of the mass $M = \sum_j \rho_j (\mathrm{d}L)^3$ for j within the region identified in Figure 6c, and compare the distribution of these local mass values across photoactivation events. Figure 6d shows the distribution of total mass within the region 2.8 Å < $|y|$ < 4.3 Å and $|x|$ < 2 Å for the first and last wait time decile for the data shown in Figure 6a,b. As with the pairwise potential energy above, the density distributions are clearly different. For the longest events the peak occurs near 115 amu, or about 10 carbon atoms. For the shortest events, the peak occurs near 95 amu or about 8 carbon atoms. Thus, the widths of the long and short-event mass distributions, σ = 36 and 31 amu, respectively, are much closer to the difference in means than in the case of the energy above. One simple measure of the predictive power is the "informedness", $J = \frac{\mathrm{TP}}{\mathrm{TP}+\mathrm{FN}} + \frac{\mathrm{TN}}{\mathrm{TN}+\mathrm{FP}} - 1$, which varies from zero for random guessing to unity for perfect classification. In this case, with an optimal division at a total mass M = 108 amu the informedness J = 0.27. For comparison, the informedness J = 0.148 when optimally partitioning the ranked pairwise potential energy at U = −5.6 kcal/mol, as shown in Figure 5b. These informedness values indicate that the local density has substantially more predictive power than the local intermolecular energy. This result is consistent with the results shown in Figure 3 which show the sample density controlling the sample-wide isomerization-time distribution.

CONCLUSIONS

In this paper, we have shown how a classical MD potential derived from ab initio quantum computations can be used in large-scale MD simulations to understand the stability of photoresponsive molecules within bulk-cooled and PVD glass samples. MD simulations scale to thousands of molecules and are fast enough to simulate glassy systems over tens of nanoseconds. Both features are orders of magnitude beyond the scales realizable with quantum calculations. With these system sizes and long simulation times comes the ability to characterize the broad, power-law distribution of isomerization wait times $P(t_f)$ over more than five decades. The power-law distribution is evident for both bulk-cooled and PVD AB samples, with a consistent power-law exponent $b \approx 1.25-1.3$. The range of the power-law behavior expands to longer time with decreasing molecular volume. Both the median and mean of the distributions fall on a single master curve with sample specific volume for the different system quench-rates, preparations, and temperature.

At the same time, the MD simulations produce extensive information about local molecule environments, which provides the opportunity to link local measures of specific volume and interaction energy to the isomerization wait time. The distributions of measures of local density and interaction energy indicate clear differences between the long and short isomerization wait time populations. Both features correlate with the wait times t_f, but the local density has more predictive power than the interaction energy. The spatial heterogeneity in the local density implies that a systematic approach to identifying local density features that correlate with response time could be an important avenue of future research.

ASSOCIATED CONTENT

Supporting Information

The Supporting Information is available free of charge at https://pubs.acs.org/doi/10.1021/acs.jpcb.0c03579.

Density and Debye-Waller factor, mean wait time versus specific volume, difference between the long and short wait-time populations data on the PVD sample densities, mean photoisomerization wait time, and local density structure (PDF)

https://dx.doi.org/10.1021/acs.jpcb.0c03579
J. Phys. Chem. B 2020, 124, 6112−6120

AUTHOR INFORMATION

Corresponding Authors

Juan J. de Pablo − *Pritzker School of Molecular Engineering, University of Chicago, Chicago, Illinois 60637, United States;* orcid.org/0000-0002-3526-516X; Email: depablo@uchicago.edu

Timothy W. Sirk − *Polymers Branch, United States Army Research Laboratory, Aberdeen Proving Ground, Maryland 21005, United States;* orcid.org/0000-0002-1105-4931; Email: timothy.w.sirk.civ@mail.mil

Authors

K. Michael Salerno − *Polymers Branch, United States Army Research Laboratory, Aberdeen Proving Ground, Maryland 21005, United States;* orcid.org/0000-0002-3667-0247

Joseph L. Lenhart − *Polymers Branch, United States Army Research Laboratory, Aberdeen Proving Ground, Maryland 21005, United States*

Complete contact information is available at: https://pubs.acs.org/10.1021/acs.jpcb.0c03579

Notes

The authors declare no competing financial interest.

ACKNOWLEDGMENTS

K.M.S. acknowledges support of an ORAU fellowship. Research was sponsored by the Army Research Laboratory and was accomplished under Cooperative Agreement Number W911NF-18-2-0105. The original support from the Army Research Office under MURI: W911NF-15-1-0568 on development of triggerable responses led to some of the concepts on light-induced softening of glasses considered here is also gratefully acknowledged. The views and conclusions contained in this document are those of the authors and should not be interpreted as representing the official policies, either expressed or implied, of the Army Research Laboratory or the U.S. Government. The U.S. Government is authorized to reproduce and distribute reprints for Government purposes notwithstanding any copyright notation herein.

REFERENCES

(1) Kearns, K. L.; Swallen, S. F.; Ediger, M. D.; Wu, T.; Yu, L. Influence of substrate temperature on the stability of glasses prepared by vapor deposition. *J. Chem. Phys.* **2007**, *127*, 154702.

(2) Swallen, S. F.; Kearns, K. L.; Mapes, M. K.; Kim, Y. S.; McMahon, R. J.; Ediger, M. D.; Wu, T.; Yu, L.; Satija, S. Organic Glasses with Exceptional Thermodynamic and Kinetic Stability. *Science* **2007**, *315*, 353−356.

(3) Kearns, K. L.; Still, T.; Fytas, G.; Ediger, M. D. High-Modulus Organic Glasses Prepared by Physical Vapor Deposition. *Adv. Mater.* **2010**, *22*, 39−42.

(4) Dawson, K. J.; Zhu, L.; Yu, L.; Ediger, M. D. Anisotropic Structure and Transformation Kinetics of Vapor-Deposited Indomethacin Glasses. *J. Phys. Chem. B* **2011**, *115*, 455−463.

(5) Qiu, Y.; Antony, L. W.; Torkelson, J. M.; de Pablo, J. J.; Ediger, M. D. Tenfold increase in the photostability of an azobenzene guest in vapor-deposited glass mixtures. *J. Chem. Phys.* **2018**, *149*, 204503.

(6) Singh, S.; de Pablo, J. J. A molecular view of vapor deposited glasses. *J. Chem. Phys.* **2011**, *134*, 194903.

(7) Singh, S.; Ediger, M. D.; De Pablo, J. J. Ultrastable glasses from in silico vapour deposition. *Nat. Mater.* **2013**, *12*, 139.

(8) Lyubimov, I.; Antony, L.; Walters, D. M.; Rodney, D.; Ediger, M. D.; de Pablo, J. J. Orientational anisotropy in simulated vapor-deposited molecular glasses. *J. Chem. Phys.* **2015**, *143*, 094502.

(9) Qiu, Y.; Antony, L. W.; de Pablo, J. J.; Ediger, M. D. Photostability Can Be Significantly Modulated by Molecular Packing in Glasses. *J. Am. Chem. Soc.* **2016**, *138*, 11282−11289.

(10) Schäfer, L. V.; Müller, E. M.; Gaub, H. E.; Grubmüller, H. Elastic Properties of Photoswitchable Azobenzene Polymers from Molecular Dynamics Simulations. *Angew. Chem., Int. Ed.* **2007**, *46*, 2232−2237.

(11) Helfferich, J.; Lyubimov, I.; Reid, D.; de Pablo, J. J. Inherent structure energy is a good indicator of molecular mobility in glasses. *Soft Matter* **2016**, *12*, 5898−5904.

(12) Paik, C. S.; Morawetz, H. Photochemical and Thermal Isomerization of Azoaromatic Residues in the Side Chains and the Backbone of Polymers in Bulk. *Macromolecules* **1972**, *5*, 171−177.

(13) Imai, Y.; Naka, K.; Chujo, Y. Isomerization Behavior of Azobenzene Chromophores Attached to the Side Chain of Organic Polymer in OrganicInorganic Polymer Hybrids. *Macromolecules* **1999**, *32*, 1013−1017.

(14) Royal, J. S.; Torkelson, J. M. Photochromic and fluorescent probe studies in glassy polymer matrices. 5. Effects of physical aging on bisphenol A polycarbonate and poly(vinyl acetate) as sensed by a size distribution of photochromic probes. *Macromolecules* **1992**, *25*, 4792−4796.

(15) Naito, T.; Horie, K.; Mita, I. Photochemistry in polymer solids: 12. Effects of main-chain structures and formation of hydrogen bonds on photoisomerization of azobenzene in various polymer films. *Polymer* **1993**, *34*, 4140−4145.

(16) Lamarre, L.; Sung, C. S. P. Studies of physical aging and molecular motion by azochromophoric labels attached to the main chains of amorphous polymers. *Macromolecules* **1983**, *16*, 1729−1736.

(17) Kondo, T.; Yoshii, K.; Horie, K.; Itoh, M. Photoprobe Study of Siloxane Polymers. 3. Local Free Volume of Polymethylsilsesquioxane Probed by Photoisomerization of Azobenzene. *Macromolecules* **2000**, *33*, 3650−3658.

(18) Naito, T.; Horie, K.; Mita, I. Photochemistry in polymer solids. 11. The effects of the size of reaction groups and the mode of photoisomerization on photochromic reactions in polycarbonate film. *Macromolecules* **1991**, *24*, 2907−2911.

(19) Glarum, S. H. Dielectric Relaxation of Polar Liquids. *J. Chem. Phys.* **1960**, *33*, 1371−1375.

(20) Mita, I.; Horie, K.; Hirao, K. Photochemistry in polymer solids. 9. Photoisomerization of azobenzene in a polycarbonate film. *Macromolecules* **1989**, *22*, 558−563.

(21) Naito, T.; Horie, K.; Mita, I. Photochemistry in polymer solids−10. Photoisomerization of 1,1-azonaphthalene in a polycarbonate film. *Eur. Polym. J.* **1990**, *26*, 1295−1300.

(22) Robertson, R. E. Effect of free volume fluctuations on polymer relaxation in the glassy state. II. Calculated results. *J. Polym. Sci., Polym. Phys.* **1979**, *17*, 597−613.

(23) Fang, G.; Maclennan, J.; Yi, Y.; Glaser, M.; Farrow, M.; Korblova, E.; Walba, D.; Furtak, T.; Clark, N. Athermal photofluidization of glasses. *Nat. Commun.* **2013**, *4*, 1521.

(24) Schoenholz, S. S.; Cubuk, E. D.; Sussman, D. M.; Kaxiras, E.; Liu, A. J. A structural approach to relaxation in glassy liquids. *Nat. Phys.* **2016**, *12*, 469.

(25) Radosz, W.; Pawlik, G.; Mitus, A. C. Complex Dynamics of Photo-Switchable Guest Molecules in All-Optical Poling Close to the Glass Transition: Kinetic Monte Carlo Modeling. *J. Phys. Chem. B* **2018**, *122*, 1756−1765.

(26) Tavarone, R.; Charbonneau, P.; Stark, H. Kinetic Monte Carlo simulations for birefringence relaxation of photo-switchable molecules on a surface. *J. Chem. Phys.* **2016**, *144*, 104703.

(27) Böckmann, M.; Peter, C.; Site, L. D.; Doltsinis, N. L.; Kremer, K.; Marx, D. Atomistic Force Field for Azobenzene Compounds Adapted for QM/MM Simulations with Applications to Liquids and Liquid Crystals. *J. Chem. Theory Comput.* **2007**, *3*, 1789−1802.

(28) Böckmann, M.; Braun, S.; Doltsinis, N. L.; Marx, D. Mimicking photoisomerisation of azo-materials by a force field switch derived from nonadiabatic ab initio simulations: Application to photo-

switchable helical foldamers in solution. *J. Chem. Phys.* **2013**, *139*, 084108.
(29) Böckmann, M.; Doltsinis, N. L. Towards understanding photomigration: Insights from atomistic simulations of azopolymer films explicitly including light-induced isomerization dynamics. *J. Chem. Phys.* **2016**, *145*, 154701.
(30) Tian, Z.; Wen, J.; Ma, J. Dynamic simulations of stimuli-responsive switching of azobenzene derivatives in self-assembled monolayers: reactive rotation potential and switching functions. *Mol. Simulat.* **2015**, *41*, 28−42.
(31) Bedrov, D.; Hooper, J. B.; Glaser, M. A.; Clark, N. A. Photoinduced and Thermal Relaxation in Surface-Grafted Azobenzene-Based Monolayers: A Molecular Dynamics Simulation Study. *Langmuir* **2016**, *32*, 4004−4015.
(32) Oostenbrink, C.; Villa, A.; Mark, A. E.; Van Gunsteren, W. F. A biomolecular force field based on the free enthalpy of hydration and solvation: The GROMOS force-field parameter sets 53A5 and 53A6. *J. Comput. Chem.* **2004**, *25*, 1656−1676.
(33) Böckmann, M.; Doltsinis, N. L.; Marx, D. Nonadiabatic Hybrid Quantum and Molecular Mechanic Simulations of Azobenzene Photoswitching in Bulk Liquid Environment. *J. Phys. Chem. A* **2010**, *114*, 745−754.
(34) Plimpton, S. Fast Parallel Algorithms for Short-Range Molecular Dynamics. *J. Comput. Phys.* **1995**, *117*, 1−19.
(35) Hockney, R.; Eastwood, J. *Computer Simulation Using Particles*; Taylor & Francis, 1988.
(36) Stillinger, F. H.; Weber, T. A. Inherent structure in water. *J. Phys. Chem.* **1983**, *87*, 2833−2840.
(37) Weber, T. A.; Stillinger, F. H. The effect of density on the inherent structure in liquids. *J. Chem. Phys.* **1984**, *80*, 2742−2746.
(38) Sciortino, F.; Kob, W.; Tartaglia, P. Inherent Structure Entropy of Supercooled Liquids. *Phys. Rev. Lett.* **1999**, *83*, 3214−3217.
(39) Bitzek, E.; Koskinen, P.; Gähler, F.; Moseler, M.; Gumbsch, P. Structural Relaxation Made Simple. *Phys. Rev. Lett.* **2006**, *97*, 170201.
(40) Lyubimov, I.; Ediger, M. D.; de Pablo, J. J. Model vapor-deposited glasses: Growth front and composition effects. *J. Chem. Phys.* **2013**, *139*, 144505.

https://dx.doi.org/10.1021/acs.jpcb.0c03579
J. Phys. Chem. B 2020, 124, 6112−6120